(12) INTERNATIONAL APPLICATION PUBLISHED UNDER THE PATENT COOPERATION TREATY (PCT)

(19) World Intellectual Property Organization
International Bureau

(43) International Publication Date
09 February 2023 (09.02.2023)

WIPO | PCT

(10) International Publication Number
WO 2023/014796 A1

(51) International Patent Classification:
G01S 15/89 (2006.01) *G01N 29/07* (2006.01)

(21) International Application Number:
PCT/US2022/039282

(22) International Filing Date:
03 August 2022 (03.08.2022)

(25) Filing Language: English

(26) Publication Language: English

(30) Priority Data:
63/229,246 04 August 2021 (04.08.2021) US

(71) Applicant: **CLOUDSTREAM MEDICAL IMAGING, INC.** [US/US]; P.O. Box 421968, Houston, Texas 77242 (US).

(72) Inventor: **PENG, Chengbin**; P.O. Box 421968, Houston, Texas 77242 (US).

(74) Agent: **SHAN, Feng**; SZDC Law PC, 1629 K Street NW, Suite 300, Washington, District of Columbia 20006 (US).

(81) Designated States *(unless otherwise indicated, for every kind of national protection available)*: AE, AG, AL, AM, AO, AT, AU, AZ, BA, BB, BG, BH, BN, BR, BW, BY, BZ, CA, CH, CL, CN, CO, CR, CU, CV, CZ, DE, DJ, DK, DM, DO, DZ, EC, EE, EG, ES, FI, GB, GD, GE, GH, GM, GT, HN, HR, HU, ID, IL, IN, IQ, IR, IS, IT, JM, JO, JP, KE, KG, KH, KN, KP, KR, KW, KZ, LA, LC, LK, LR, LS, LU, LY, MA, MD, ME, MG, MK, MN, MW, MX, MY, MZ, NA, NG, NI, NO, NZ, OM, PA, PE, PG, PH, PL, PT, QA, RO, RS, RU, RW, SA, SC, SD, SE, SG, SK, SL, ST, SV, SY, TH, TJ, TM, TN, TR, TT, TZ, UA, UG, US, UZ, VC, VN, WS, ZA, ZM, ZW.

(84) Designated States *(unless otherwise indicated, for every kind of regional protection available)*: ARIPO (BW, GH, GM, KE, LR, LS, MW, MZ, NA, RW, SD, SL, ST, SZ, TZ, UG, ZM, ZW), Eurasian (AM, AZ, BY, KG, KZ, RU, TJ, TM), European (AL, AT, BE, BG, CH, CY, CZ, DE, DK, EE, ES, FI, FR, GB, GR, HR, HU, IE, IS, IT, LT, LU, LV, MC, MK, MT, NL, NO, PL, PT, RO, RS, SE, SI, SK, SM, TR), OAPI (BF, BJ, CF, CG, CI, CM, GA, GN, GQ, GW, KM, ML, MR, NE, SN, TD, TG).

(54) Title: INVERSION OF SOUND SPEED AND POISSON'S RATIO FROM ULTRASOUND BEAM DATA FOR CHARACTERIZATION OF TISSUES

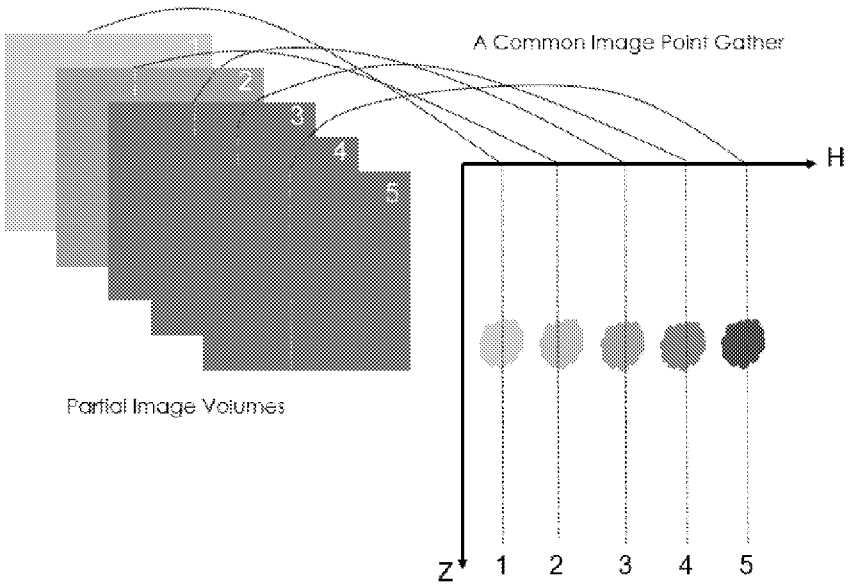

FIG. 2

(57) Abstract: A method for obtaining a sound speed image is disclosed. A reflectivity value and a sound speed value at every image point are obtained at the same time. Together they can be used to perform more detailed characterization of tissues and organs under examination. A method for obtaining a spatially varying Poisson's ratio distribution is also disclosed. A reflectivity value and a Poisson's ratio value at every image point are obtained at the same time. Together they can be used to perform more detailed characterization of tissues and organs under examination.

[Continued on next page]

WO 2023/014796 A1

Published:
— *with international search report (Art. 21(3))*

INVERSION OF SOUND SPEED AND POISSON'S RATIO FROM ULTRASOUND BEAM DATA FOR CHARACTERIZATION OF TISSUES

This application claims priority to US Provisional Patent Application No. 63/229,246, filed on August 4, 2021, which is incorporated by reference for all purposes as if fully set forth herein.

FIELD OF THE INVENTION

[0001] The present invention relates to a method for obtaining a sound speed image and a Poisson's ratio image for characterization of the tissues.

BACKGROUND OF THE INVENTION

[0002] An ultrasound scanner produces pictures of the inside of human body using sound waves. It uses a small probe called a transducer placed directly on the skin. High-frequency sound waves travel from the probe into the body. The probe collects sound reflections that bounce back from acoustic contrasts in tissues and organs. Ultrasound signals contain information about mechanical and acoustic properties of tissues and organs through which the ultrasound waves propagate or from which ultrasound waves are reflected. Those sound waves are used to create an image. Ultrasound imaging is a noninvasive medical test that helps a physician to diagnose and treat medical conditions [1, 2].

[0003] Medical ultrasound applications need to make a step change from general diagnostic imaging to quantitative characterization of tissues and organs. Seeing a feature on an ultrasound image is one thing. Knowing what is inside the feature is another thing. The latter ought to be more useful for clinical applications. In this way we can make ultrasound imaging technologies more competitive with or complementary to X-CT and MRI modalities. Attempts were made to measure physical properties of tissues using ultrasound. Shear wave elastography was an example. It uses shear wave fronts excited by a moving focused ultrasound beam to measure shear wave speeds in tissues [3, 4]. Travel time tomography was also used to invert for compressional wave velocities in tissues. It uses the travel time of sound waves between a pair of transmitter and receiver [5, 6]. Diffraction tomography was used for breast imaging. It uses diffracted waves to invert for compressional wave speed distribution in breast tissues [7]. Recently deep learning and artificial intelligence methods were used to invert for sound speed in medical ultrasound, using computer generated synthetic ultrasound data as training dataset since a large amount of training datasets is hard to come by [8]. Full waveform inversion was also reported in literature where a super-

computer was used to invert for sound speed variations by exactly matching recorded waveforms with computer generated waveforms [9, 10].

[0004] Commercial ultrasound scanners are good at producing a diagnostic image to show shapes and structures of tissues and organs under examination. The images could not tell other important properties that are needed to characterize the health of the tissues, such as, hardness of the tissues, density, sound speed, Poisson's ratio, mechanical moduli, water content, to name a few. Clinic physicians want to know more about features and lesions seen on an ultrasound image.

SUMMARY OF THE INVENTION

[0005] The present invention relates to ultrasound imaging in general. In particular, the invention extends ultrasound to detailed characterization of physical properties of tissues and organs. In one way we can obtain not only a reflectivity image (B-mode image) but also the sound speed value at every image point at the same time. The B-mode reflectivity image and sound speed image together can be used to perform more detailed characterization of tissues and organs under examination. B-Mode is a two-dimensional ultrasound image display composed of bright dots representing ultrasound echoes with brightness proportional to echo strength.

[0006] In another way we can obtain not only a reflectivity image but also Poisson's ratio value at every image point at the same time. Poisson's ratio is an important material property. The value of Poisson's ratio is 0.5 for water, or slightly less than 0.5 for soft tissues that contain a lot of water in content. Muscular tissues have Poisson's ratio in the range of 0.30 - 0.45. Bones have Poisson's ratio values in the range of 0.35 - 0.4. Kidney stones have even smaller Poisson's ratio values (< 0.3). The B-mode reflectivity image and the Poisson's ratio image together can be used to perform more detailed characterization of tissues and organs under examination.

[0007] In one embodiment, the present application discloses a method for obtaining a sound speed image, and the method includes the steps of: (1) spraying, with a processor, a data sample of an ultrasound beam, measured with an apparatus that contains an ultrasound array transducer, into an image space of a subject along an impulse response curve; (2) collecting, with the processor, contributions of the data sample in the image space; (3) summing contributions of a plurality of data samples by repeating the step (1) and the step (2) for a plurality of ultrasound beams, with the processer, to generate a plurality of partial images, and storing the partial images in a first memory location; (4) sorting, with the processor, the partial images to form common image point gathers at a plurality of spatial

locations, and storing the common image point gathers in a second memory location; (5) measuring, with the processor, residual moveout values on the common image point gathers, each residual moveout value relating to a corresponding spatial location; and (6) inverting, with the processor, the residual moveout values to form an image of the sound speed, and sending the sound speed image to a net address via TCP/IP, a display port on a host computer, or a third memory location.

[0008] In another embodiment, the step (6) includes: setting an initial sound speed; and calculating, with the processor, an updated sound speed value at the corresponding spatial location using the initial sound speed and the each residual moveout value.

[0009] In another embodiment, the initial sound speed is 1,540 m/s.

[0010] In another embodiment, the step (6) further includes: applying a spatial smoothing, with the processor, to the sound speed image to remove rapid variations.

[0011] In another embodiment, the present application provides a method for obtaining a Poisson's ratio image, and the method includes the steps of: (1) spraying, with a processor, a data sample of an ultrasound beam, measured with an apparatus that contains an ultrasound array transducer, into an image space of a subject along an impulse response curve; (2) collecting, with the processor, contributions of the data sample in the image space; (3) summing the contributions of a plurality of data samples by repeating the step (1) and the step (2) for a plurality of ultrasound beams, with the processer, to generate a plurality of partial images, and storing the partial images in a first memory location; (4) sorting, with the processor, the partial images to form common image point gathers at a plurality of spatial locations, and storing the common image point gathers in a second memory location; (5) measuring, with the processor, residual moveout values on the common image point gathers, each residual moveout value relating to a corresponding spatial location; (6) applying, with the processor, residual moveout corrections to flatten the common image point gathers; (7) measuring, with the processor, amplitudes and reflection angles on the common image point gathers, each pair of amplitude and reflection angle relating to a corresponding spatial location; and (8) inverting, with the processor, the amplitudes and reflection angles to form a Poisson's ratio image, and sending the Poisson's ratio image to a net address via TCP/IP, a display port on a host computer, or a third memory location.

[0012] In another embodiment, the step (8) comprises: estimating a normal incident reflection amplitude; and calculating, with the processor, a proxy of Poisson's ratio at the corresponding spatial location using the normal incident reflection amplitude and the measured amplitudes at a plurality of reflection angles.

[0013] In another embodiment, the step (8) comprises: estimating a normal incident reflection amplitude; and calculating, with the processor, a proxy of shear wave speed contrast at the corresponding spatial location using the normal incident reflection amplitude and the measured amplitudes at a plurality of reflection angles.

[0014] It is to be understood that both the foregoing general description and the following detailed description are exemplary and explanatory and are intended to provide further explanation of the invention as claimed.

BRIEF DESCRIPTION OF THE DRAWINGS

[0015] The accompanying drawings, which are included to provide a further understanding of the invention and are incorporated in and constitute a part of this specification, illustrate embodiments of the invention and together with the description serve to explain the principles of the invention.

[0016] In the drawings:

[0017] Figure 1 shows finite support [X_{min}, X_{max}] of a Beam Impulse Response Curve. An impulse response of a beamforming operator is a curve (thick line) that contains all possible image points that one sample in a beam record contributes to. The open circle is the focus for this beam with a T_x aperture (of active transmitters) and a R_x aperture (of active receivers). The solid black dot at (x, z) is an output image point. Here X_c is the beam center coordinate. X_r is the receiver coordinate for this data sample. X_s is the stationary phase solution of the effective transmitter coordinate. Offset H is the distance between X_r and X_s. Reflection angle is half of the intersection angle between a line from X_s to (x, z) and another line from X_r to (x, z). Top (I) is for the case $Z < Z_F$. Bottom (II) is for the case $Z > Z_F$.

[0018] Figure 2 shows the formation of a common image point gather: at each fixed lateral position we extract one vertical trace from each partial image volume and put them side by side. This organization of beamformed partial images is called a common image point gather. The vertical axis is image depth or two-way vertical time. The horizontal axis is the binning attribute used in formation of the partial images. We use the index number of each partial image volume in this illustration. We can also use the physical value of the binning attribute to label the horizontal axis.

[0019] Figure 3 shows residual moveout curvatures on common image point gathers: the left panel has negative curvature, indicating $V_0 < V_{RMS}$; the middle panel has zero curvature, indicating $V_0 = V_{RMS}$; the right panel has positive curvature, indicating $V_0 > V_{RMS}$.

[0020] Figure 4 shows two published B-mode images on USTB website (www.ustb.no) of PICMUS carotid challenge dataset: (left) a transversal image of neck

artery, and (right) a longitudinal image of the same. All displays are in 60 dB with log compression, with white color representing bright (high) amplitudes and black color for dim (low) amplitudes.

[0021] Figure 5 shows two B-mode images obtained with our method using the PICMUS carotid challenge dataset as input: (left) a transversal image of neck artery, and (right) a longitudinal image of the same. All displays are in 60 dB with log compression, with white color representing bright (high) amplitudes and black color for dim (low) amplitudes.

[0022] Figure 6 show common image point gathers obtained with our method using the PICMUS carotid challenge dataset. Each panel shows a common image point gather at a given lateral location. Within each gather the vertical axis is depth and the horizontal axis is transmitter-receiver offset.

[0023] Figure 7 shows a sound speed image using the PICMUS carotid challenge dataset: (left) a transversal view in sound speed of neck artery, and (right) a longitudinal view of the same. The color bar is in m/s.

[0024] Figure 8 shows a Poisson's ratio (proxy) image using the PICMUS carotid challenge dataset: (left) a transversal view of neck artery, and (right) a longitudinal view of the same.

[0025] Figure 9 shows main components of an apparatus for imaging sound speed property of tissues, and the apparatus includes an ultrasound array transducer that transmits and receives echo data and one or more GPU processors that (1) sprays data samples of ultrasound beams into the image space along their impulse response curves, (2) collects image contributions of all data samples to generate a plurality of partial images, (3) stores the partial images in a first memory location, (4) sorts the partial images into a plurality of common image point gathers, (5) stores the common image point gathers in a second memory location, (6) measures residual moveout values at a plurality of spatial locations, and (7) inverts the residual moveout values to obtain a sound speed image. The apparatus also includes a host computer that sends the sound speed image to a net address via TCP/IP, or a display port on the host computer, or a third memory location for further processing.

[0026] Figure 10 shows main components of an apparatus for imaging Poisson's ratio (proxy) property of tissues, and the apparatus includes an ultrasound array transducer that transmits and receives echo data and one or more GPU processors that (1) sprays a data sample of an ultrasound beam into the image space along its impulse response, (2) collects image contributions of all data samples to generate a plurality of partial images, (3) stores the partial images in a first memory location, (4) sorts the partial images into a plurality of

common image point gathers, (5) stores the common image point gathers in a second memory location, (6) measures residual moveout values at a plurality of spatial locations, (7) applies residual moveout corrections on common image point gathers, (8) measures reflection amplitudes and reflection angles at a plurality of spatial locations, and (9) inverts the pairs of amplitude and reflection angle data to obtain a Poisson's ratio (proxy) image. The apparatus also includes a host computer that sends the Poisson's ratio (proxy) image to a net address via TCP/IP, or a display port on the host computer, or a third memory location for further processing.

DETAILED DESCRIPTION OF THE ILLUSTRATED EMBODIMENTS

[0027] Reference will now be made in detail to embodiments of the present invention, example of which is illustrated in the accompanying drawings.

[0028] Traditional beamforming of ultrasound data utilizes dynamic focusing method implemented on FPGA hardware [1, 2]. Modern ultrasound imaging applications use pixel-based beamforming methods [11 – 16], mostly implemented on GPU hardware. All these methods can be easily understood by examining spatial impulse responses of the beamforming operators applied on individual data sample collected by an ultrasound scanner. An impulse response of a beamforming operator, by our definition, is a curve in image domain with a finite support. It contains all possible image points that one data sample in one input ultrasound beam contributes to. The final image is formed by summing all impulse responses for all data samples of all input beams. Figure 1 depicts one impulse response for a focused beam (thick black curve). Similar impulse responses can be produced for a divergent beam and a planewave beam. In Figure 1 an acquisition layout for one input beam is shown. Active transmitters are covered by the short dash line labeled Tx aperture. Active receivers are covered by the long dash line labeled Rx aperture. These two apertures can be the same or different without any impact on our analysis herein. The leftmost transmitter is at X_{sL} and the rightmost transmitter is at X_{sR}. The beam center is at X_c. The focal point is at (X_F, Z_F). One time sample recorded by a receiver at X_r is used to produce the impulse response curve. The impulse response curve has a finite support between $[X_{min}, X_{max}]$ beyond which there are no stationary reflections for this data sample. This physical restriction is ignored by all published pixel-based beamforming methods. It is also worthwhile to note that the traditional dynamic focusing method corresponds to a single point on the impulse response curve at the location where the curve intersects with the scanline of this beam. In this regard the dynamic focusing method is wasteful in utilizing the ultrasound beam data for imaging because only one point is imaged by a whole beam.

[0029] Formulas are given in the box in Figure 1 for the calculation of the impulse response and its spatial support. X_s is the stationary location of a transmitter that makes a significant contribution to the image at the output point (x, z). The distance between X_s and X_r is called the stationary offset, or simply offset. The reflection angle at (x, z) is called the stationary specular reflection angle, or simply reflection angle. Each point on the impulse response curve carries distinct values of offset, reflection angle, dip angle, to name a few. Partial image volumes can be generated by binning and sorting each point on the impulse response curve according to the value of offset, reflection angle, or some other attribute. In the box, t_a is the travel time from the receiver to the image point, t_b is the travel time from the focal point to the image point, and t_c is the travel time from the focal point to the beam center. The arrival time of the input data sample is t.

[0030] A general formulation of impulse responses for ultrasound beam data of arbitrary types can be found in our separate patent application, US. Provisional Patent Application No. 63/184174, filed May 4, 2021.

[0031] A common image point gather is formed by sorting all partial images at a fixed output location into a gather as shown in Figure 2. A partial image volume is generated, during beamforming, by binning and sorting each point on an impulse response curve according to the value of offset, reflection angle, or some other attribute. The final image is formed by stacking common image point gathers at every output location.

[0032] It is worthwhile to note that, if the correct sound speed is used in beamforming, the common image point gather in Figure 2 should be flat. These partial images will coherently compound together to form an enhanced image with good resolution and good signal to noise ratio. A detailed description of common image point gathers of ultrasound beam data can be found in our separate patent application, US Provisional Patent Application No. 63/197932, Filed Jun 7, 2021.

[0033] Inversion for Spatially Varying Sound Speed

[0034] Residual Moveout Analysis

[0035] The best sound speed value that yields a focused image of ultrasound data at a given spatial location is the RMS (root-mean-square) equivalent of the true sound speed distribution in tissues that acoustic waves travel through. Sound speed varies spatially in tissues, either continuously or in a discontinuous fashion. The RMS equivalent of sound speed, at a given location, is given by:

$$V_{RMS}{}^2(T) = \frac{1}{T}\int_0^T V^2(t)\,dt \qquad (1)$$

where V(t) is a sound speed profile that is converted into vertical two-way time.

[0036] If the sound speed value used in beamforming (V_0) is equal to the effective sound speed value (V_{RMS}) in equation (1), then all partial images should be spatially co-located (i.e., the same tissue structure is imaged multiple times from different illuminations). In this case one should see a flat common image point gather for reflection data at every output location (Figure 3, middle). Non-flat common image point gathers indicate that the sound speed value used in beamforming is not optimal for reflection data, either a wrong value is chosen or the actual sound speed in tissues is spatially varying such that a constant value could not represent the true sound speed variation inside a human body. In the case $V_0 < V_{RMS}$ residual moveout curvature is negative (Figure 3, left). In the case $V_0 > V_{RMS}$ residual moveout curvature is positive (Figure 3, right). Therefore, residual moveout curvatures on common image point gathers can be used to invert for sound speed distribution in the image domain.

[0037] The correct sound speed value V_1 (RMS equivalent) that yields the best focused images at a given spatial location is related to the residual moveout curvature according to the following formula:

$$\frac{1}{V_1^2} = \frac{1}{V_0^2} + \frac{1}{V_{RMO}^2} \quad (2)$$

where V_0 is the sound speed used in an initial beamforming (typically 1540 m/s). V_{RMO} is the inverse of the residual moveout curvature we measure on a common image point gather. If the gather is flat, i.e., the curvature term is zero, the second term in the right-hand side of equation (2) vanishes. This leads to $V_1 = V_0$. If the residual moveout curvature is positive, we will have $V_1 < V_0$. If the residual moveout curvature is negative, we will have $V_1 > V_0$.

[0038] The Dix Inversion

[0039] The Dix inversion formula has not been used in B-mode ultrasound imaging for medical applications. The inversion formula proposed by Dix [19] is given as:

$$V^2(T_1, T_2) = \frac{T_2 V_{RMS}^2(T_2) - T_1 V_{RMS}^2(T_1)}{T_2 - T_1} \quad (3)$$

where $V(T_1, T_2)$ is the estimated average sound speed between two-way vertical time T_1 and T_2. Inputs to the Dix inversion are RMS equivalent sound speeds at the time samples.

[0040] The Dix inversion is one dimensional in nature and its result looks blocky between data points. Editing out some outliers and applying some spatial smoothing are common practices in geophysical applications [20].

[0041] Inversion for Spatially Varying Poisson's Ratio

[0042] The use of amplitude information (or echo strength) in B-mode ultrasound imaging is mostly for identification of echoic regions and anechoic regions in human bodies. We extend the use of amplitude measurements on common image point gathers to directly invert or infer physical property distributions in tissues, such as Poisson ratio, Young's moduli, compressional impedance, shear impedance, density, water content, to name a few. The data used in our inversion or inference are pairs of amplitudes and reflection angles (or offsets) measured on common image point gathers [21, 22]. The methodology is not known in medical applications such as B-mode ultrasound imaging.

[0043] If contrasts in acoustic properties across an internal boundary are small, the reflection amplitudes vary with the reflection angles according to the following formula:

$$R(\theta) = A + B \sin^2\theta \tag{4}$$

where A is the normal incidence reflection amplitude and B is the gradient in a cross plot of amplitude $R(\theta)$ and $\sin^2\theta$. In a linearized approximation they are related to contrasts in physical parameters as follows [23, 24]:

$$A = \frac{1}{2}\left(\frac{\Delta V}{V} + \frac{\Delta\rho}{\rho}\right) \tag{5a}$$

$$B = -\frac{3-7\sigma}{2(1-\sigma)}\frac{\Delta V}{V} - \frac{1-2\sigma}{(1-\sigma)}\frac{\Delta\rho}{\rho} + \frac{1}{(1-\sigma)^2}\Delta\sigma \tag{5b}$$

where V is sound speed (compressional wave), ρ is density, and σ is Poisson's ratio. $\frac{\Delta V}{V}$ is the relative change of sound speed across an internal boundary. $\frac{\Delta\rho}{\rho}$ is the relative change of density. $\Delta\sigma$ is the absolute change of Poisson's ratio.

[0044] Human tissues are 90% or more water in content. Values of Poisson's ratio in human tissues are close to 0.5 which is the Poisson's ratio of water. In this case the first two terms of B in equation (2b) are much smaller than the third term. The gradient B is mostly related to the contrast in Poisson's ratio σ for medical ultrasound applications. We shall call the gradient B a proxy of Poisson's ratio in these cases. In all examples below we are using the gradient B value as a proxy of Poisson's ratio attribute in our analysis.

[0045] In human tissues the relative change of compressional wave speed is much smaller than the relative change of shear wave speed, i.e., $\left|\frac{\Delta V}{V}\right| \ll \left|\frac{\Delta V_S}{V_S}\right|$. It is easy to show that:

$$\frac{\Delta V_S}{V_S} = -\frac{1}{2(1-\sigma)(1-2\sigma)}\Delta\sigma \tag{6}$$

[0046] Therefore, the gradient B is also negatively correlated with the relative change of shear wave speed:

$$B = -\frac{2(1-2\sigma)}{(1-\sigma)}\frac{\Delta V_S}{V_S} \quad (7)$$

[0047] The significance of equation (7) is that we can obtain shear wave information using B-mode ultrasound beam data without actual excitation of shear waves in tissues, which is different from shear wave elastography [3, 4].

[0048] The Poisson's ratio proxy (also shear wave reflectivity proxy) can be obtained from a parametric fitting / linear regression of equation (4) on a common image point gather on which both reflection amplitudes and reflection angles are measured. We first compute envelopes of traces on the common image point gather in order to remove the impact of wavelet polarity on the regression or fitting. We then perform the two parameters (A and B) regression using the envelope amplitudes. The resulting B value is a good indication how amplitudes vary with reflection angles: a positive B value corresponds to the case of the envelope amplitude increasing with reflection angle; a negative B value corresponds to the case of the envelope amplitude decreasing with reflection angle. We repeat this process for all output locations to obtain an image of the Poisson's ratio proxy (i.e., B value). The image can also be interpreted as a proxy of the shear wave reflectivity.

[0049] Positive B values are typically associated with soft tissues with a lot of water content (σ *is close to* 0.5). Negative B values are typically associated with harder or solid tissues with less water content ($\sigma < 0.45$) . The B value (Poisson's ratio proxy) is sensitive to water content, which shares similarity with MRI images used by clinical physicians. It is also sensitive to calcification of tissues (such as liver) where the values of Poisson's ratio decrease and the values of shear wave speed increase significantly.

[0050] ***In Vivo*** **Carotid Ultrasound Data Example**

[0051] PICMUS Carotid Challenge Data

[0052] PICMUS is the IEEE US 2016 Plane-wave Imaging Challenge in Medical UltraSound, an initiative of IEEE US to promote use of plane-wave ultrasound imaging modality. PICMUS carotid challenge dataset is a public domain dataset for download at Ultrasound Test Benchmark (USTB) website (https://www.ustb.no/ustb-datasets). The dataset contains two in vivo carotid scans, one in the cross section and another in longitudinal section, collected by a volunteer with a Verasonics Vantage 256 System and a Verasonics L11 transducer. The use of this dataset is subject to citation rule (https://www.ustb.no/examples/picmus/picmus-invivo-carotid-cross and https://www.ustb.no/examples/picmus/picmus-invivo-carotid-long). We sincerely thank IEEE US for making this dataset available in the public domain.

[0053] The images in Figure 5 are published B-mode images on USTB website for benchmark purposes. The raw ultrasound data is collected in two directions, one measurement (left) is in a direction transversal to the neck artery in-vivo, and the other measurement (right) is in a longitudinal direction. Bright colors represent stronger acoustic echoes when an ultrasound beam is reflected from tissue contrasts in acoustic impedance. Darker regions are anechoic, with much smaller acoustic contrasts. Public are encouraged to produce better results with improved algorithms.

[0054] Enhanced B-Mode Images

[0055] We are able to produce improved images with the method disclosed in this invention, using the same PIMCUS carotid raw ultrasound data as input. Figure 6 shows our results: improvements can be seen in both contrast resolution and spatial resolution, with clear definition of walls of carotid artery (circular features on the left and elongated features on the right), showing no build-up of fatty deposits on the vessel walls. The dark regions are either anechoic or acoustic waves being strongly attenuated during wave propagation (e.g., near the bottom).

[0056] Sound Speed Images

[0057] To obtain a spatially varying sound speed image we first generate a set of common image point gathers using the PICMUS carotid challenge dataset. Since sound waves in different tissues propagate with different speed values, a beamforming algorithm that uses a constant value for sound speed will always produce non-flat common image point gathers as shown in Figure 7. The residual moveout on the common image point gathers can be accurately measured. The Dix inversion is then applied to obtain sound speed distribution in the image domain. Figure 7 shows resulting sound speed images: the left one is a sound speed image in the transversal direction, and the right one is another sound speed image in the longitudinal direction. One can see lower sound speed values inside the carotid vessels. Soft tissues also have lower sound speed values. Muscle tissues have higher sound speed values. Since the Dix inversion is a 1-D method we typically see vertical stripes in the output. One can apply a spatial smoothing to remove the vertical stripes, if desired.

[0058] It is worthwhile to note that the estimated values of sound speed at the bottom part of the images are not reliable as acoustic waves are strongly attenuated by tissue absorption before they can reach the transducer placed on the top surface (dark color in Figure 7). We can cut out the deep portion, if desired. Figure 9 is a schematic diagram of the method and the apparatus for obtaining a sound speed image.

[0059] Poisson's Ratio Images

[0060] To obtain an image of spatially varying Poisson's ratio we generate a set of common image point gathers using the PICMUS carotid challenge dataset. We measure the residual moveouts on the common image point gathers. We perform a residual moveout correction to flatten the common image point gathers. We measure amplitudes on the common image point gathers and estimate B values using the amplitude vs. sine squared reflection angle cross-plot. The B value serves as a proxy of Poisson's ratio (also a good proxy of shear wave reflectivity). Fluid and fatty tissues have larger Poisson's ratio value. Muscle tissues and bones have smaller Poisson's ratio value. Therefore, we can use the Poisson's ratio value to aid our characterization of various tissues. Figure 8 shows resulting Poisson's ratio (proxy) images: the left one is an image of Poisson's ratio (proxy) in the transversal direction, and the right one is another image in the longitudinal direction. One can see higher Poisson's ratio values (light gray color) inside the carotid artery (fluid) and soft tissues. In muscular tissues the Poisson's ratio values are smaller (dark region). The Poisson's ratio (proxy) image is useful in delineating body fluids and fatty tissues. Figure 10 is a schematic diagram of the method and the apparatus for obtaining a Poisson's ratio image.

[0061] It will be apparent to those skilled in the art that various modifications and variations can be made in the present invention without departing from the spirit or scope of the invention. Thus, it is intended that the present invention cover the modifications and variations of this invention provided they come within the scope of the appended claims and their equivalents.

References

[1] Richard S. C. Cobbold (2007), Foundations of Biomedical Ultrasound, Oxford University Press, pages 1416-1428.

[2] F. W. Kremkau (2006), Diagnostic Ultrasound: Principles and Instruments, 7th edition, Saunders/ Elsevier, St. Louis.

[3] J. Ophir, S. K. Alam, B. S. Garra, F. Kallel, E. E. Knonfgou, T. Krousko, and C. R. B. Berritt (2002), Elastography: Imaging the Elastic Properties of Soft Tissues with Ultrasound, J. Medical Ultrasonics, Vol 29, pages 155 – 171.

[4] J. Bercoff, M. Tanter, T. M. Nguyen, J. M. Chassot, M. Fink, and C. Boccara (2004), Supersonic Shear Imaging: A New Technique for Soft Tissue Elasticity Mapping, IEEE Trans. On Ultrasonics, Ferroelectrics and Frequency Control, Vol 51, pages 396 – 409.

[5] M. Sak, N. Duric, P. Littrup, L. Bey-Knight, H. Ali, P. Vallieres, M. E. Sherman and G. L. Gierach (2017), Using Speed of Sound Imaging to Characterize Breast Density, Ultrasound in Medicine & Biology, Vol 43, pages 91 – 103.

[6] C. Li, A. Stewart and N. Duric (2012), Multi-grid Tomographic Inversion for Breast Ultrasound Imaging, Proceedings of SPIE, Vol 8320, pages 1-9.

[7] J. Nebeker and T. R. Nelson (2012), Imaging of Sound Speed Using Reflection Ultrasound Tomography, Journal of Ultrasound in Medicine, Vol 31, pages 1389 – 1404.

[8] Micha Feigin, D. Freedman, and B. W. Anthony, A Deep Learning Framework for Single-Sided Sound Speed Inversion in Medical Ultrasound, IEEE Transactions on Biomedical Engineering, Vol. 67, pages 1142– 1150.

[9] J. Wiskin, B. Malik, D. Borup, N. Pirshafiery and J. Klock (2020), Full Wave 3D Inverse Scattering Transmission Ultrasound Tomography in the Presence of High Contrast, Nature, https://doi.org/10.1038/s41498-020-76754-3.

[10] L. Guasch, O. Calderon-Agudo, M. X. Tang, P. Nachev, and M. Warner (2020), Full-waveform Inversion Imaging of the Human Brain, Nature, https://doi.org/10.1038/s41746-020-0240-8.

[11] R. E. Daigle (2009), Ultrasound Imaging System with Pixel Oriented Processing, U.S. Patent Application No. 2009/0112095 A1, April 30, 2009.

[12] R. Zemp and M. F. Insana (2007), Imaging with Unfocused Regions of Focused Ultrasound Beams, J. Acoust. So. Amer. Vol. 121, pages 1491-1498.

[13] N. Q. Nguyen and Richard Q. Prager (2016), High-resolution Ultrasound Imaging with Unified Pixel-Based Beamforming, IEEE Transactions on Medical Imaging, Vol. 35, pages 98-108.

[14] O. M. H. Rindal (2019), Software Beamforming in Medical Ultrasound Imaging – a Blessing and a Curse, Ph.D. Thesis, University of Oslo.

[15] O. M. H. Rindal, A. Rodriguez-Molares, and A. Austeng (2018), A Simple, Artifact-free, Virtual Source Model, IEEE International Ultrasonics Symposium, IUS 1-4. https:://doi.org/10.1109/ultsym.2018.8579944.

[16] D. J. Napolitano, B. D. DeBusschere, G. W. McLaughlin, L. Y. Mo, C. H. Chou, T. L. Ji, R. W. Steins (2011), Continuous Transmit Focusing Method and Apparatus for Ultrasound Imaging Systems, US Patent 8,002,705, Issued Aug, 2011.

[17] C. Peng and J. Tang (2021), Acquisition and Processing of V-Wave Ultrasound Data Using a Linear or Curved Array Transducer, US. Patent Appl No. 63/184174, Filed May 4, 2021.

[18] C. Peng, and J. Tang (2021), Imaging Tissues and Organs Behind Bones Using an Ultrasound Array Transducer, US Patent Appl No. 63/197932, Filed Jun 7, 2021.

[19] C. H. Dix (1955), Seismic Velocities from Surface Measurements, Geophysics, Vol. 20, pages 68 – 86.

[20] Z. Koren and I. Ravve (2006), Constrained Dix Inversion, Geophysics, Vol. 71, pages R113 – R130.

[21] K, Aki and P. G. Richards (1980), Quantitative Seismology: Theory and Methods, W. H. Freeman and Co.

[22] O. Yilmaz (2011), Seismic Data Analysis: Processing, Inversion and Interpretation of Seismic Data, Society of Exploration Geophysicists.

[23] R. Bortfeld (1961), Approximation to the Reflection and Transmission Coefficients of Plane Longitudinal and Transverse Waves, Geophysical Prospecting, Vol 9, pages 485 – 503.

[24] J. P. Castagna, H. W. Swan, and D. J. Foster (1998), Framework for AVO Gradient and Intercept Interpretation, Geophysics, Vol 63, pages 948 – 956.

WHAT IS CLAIMED IS:

1. A method for obtaining a sound speed image, comprising the steps of:

(1) spraying, with a processor, a data sample of an ultrasound beam, measured with an apparatus that contains an ultrasound array transducer, into an image space of a subject along an impulse response curve;

(2) collecting, with the processor, contributions of the data sample in the image space;

(3) summing contributions of a plurality of data samples by repeating the step (1) and the step (2) for a plurality of ultrasound beams, with the processer, to generate a plurality of partial images, and storing the partial images in a first memory location;

(4) sorting, with the processor, the partial images to form common image point gathers at a plurality of spatial locations, and storing the common image point gathers in a second memory location;

(5) measuring, with the processor, residual moveout values on the common image point gathers, each residual moveout value relating to a corresponding spatial location; and

(6) inverting, with the processor, the residual moveout values to form an image of the sound speed, and sending the sound speed image to a net address via TCP/IP, a display port on a host computer, or a third memory location.

2. The method of claim 1, wherein the step (6) comprises:

setting an initial sound speed; and

calculating, with the processor, an updated sound speed value at the corresponding spatial location using the initial sound speed and the each residual moveout value.

3. The method of claim 2, wherein the initial sound speed is 1,540 m/s.

4. The method of claim 2, wherein the step (6) further comprises:

applying a spatial smoothing, with the processor, to the sound speed image to remove rapid variations.

5. A method for obtaining a Poisson's ratio image, comprising the steps of:

(1) spraying, with a processor, a data sample of an ultrasound beam, measured with an apparatus that contains an ultrasound array transducer, into an image space of a subject along an impulse response curve;

(2) collecting, with the processor, contributions of the data sample in the image space;

(3) summing the contributions of a plurality of data samples by repeating the step (1) and the step (2) for a plurality of ultrasound beams, with the processer, to generate a plurality of partial images, and storing the partial images in a first memory location;

(4) sorting, with the processor, the partial images to form common image point gathers at a plurality of spatial locations, and storing the common image point gathers in a second memory location;

(5) measuring, with the processor, residual moveout values on the common image point gathers, each residual moveout value relating to a corresponding spatial location;

(6) applying, with the processor, residual moveout corrections to flatten the common image point gathers;

(7) measuring, with the processor, amplitudes and reflection angles on the common image point gathers, each pair of amplitude and reflection angle relating to a corresponding spatial location; and

(8) inverting, with the processor, the amplitudes and reflection angles to form a Poisson's ratio image, and sending the Poisson's ratio image to a net address via TCP/IP, a display port on a host computer, or a third memory location.

6. The method of claim 5, wherein the step (8) comprises:

estimating a normal incident reflection amplitude; and

calculating, with the processor, a proxy of Poisson's ratio at the corresponding spatial location using the normal incident reflection amplitude and the measured amplitudes at a plurality of reflection angles.

7. The method of claim 5, wherein the step (8) comprises:

estimating a normal incident reflection amplitude; and

calculating, with the processor, a proxy of shear wave speed contrast at the corresponding spatial location using the normal incident reflection amplitude and the measured amplitudes at a plurality of reflection angles.

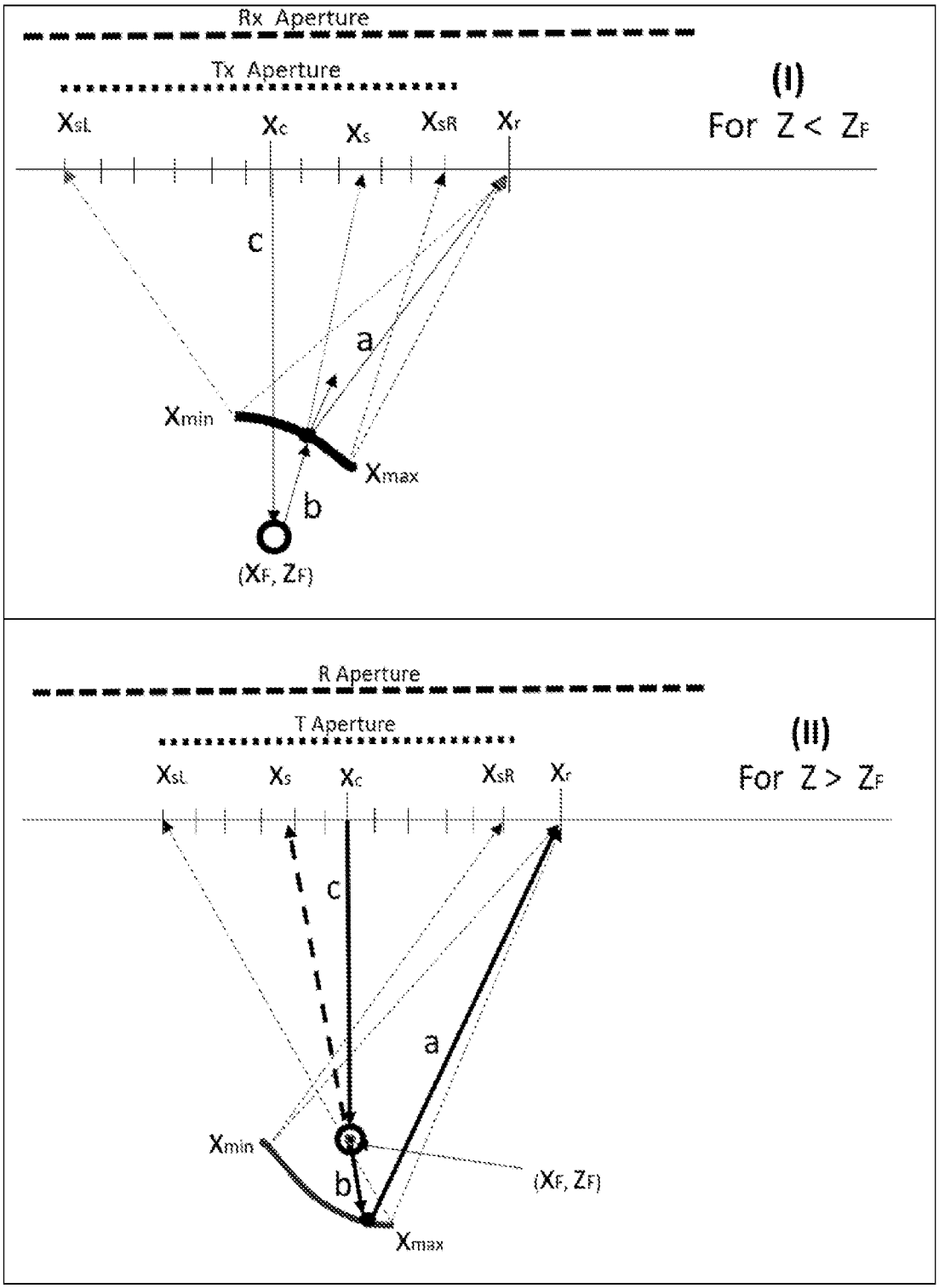
Rx Aperture
Tx Aperture
(I)
For Z < ZF
XsL
Xc
Xs
XsR
Xr
c
a
Xmin
Xmax
b
(XF, ZF)
R Aperture
T Aperture
(II)
For Z > ZF
XsL
Xs
Xc
XsR
Xr
c
a
Xmin
b
(XF, ZF)
Xmax

FIG. 1

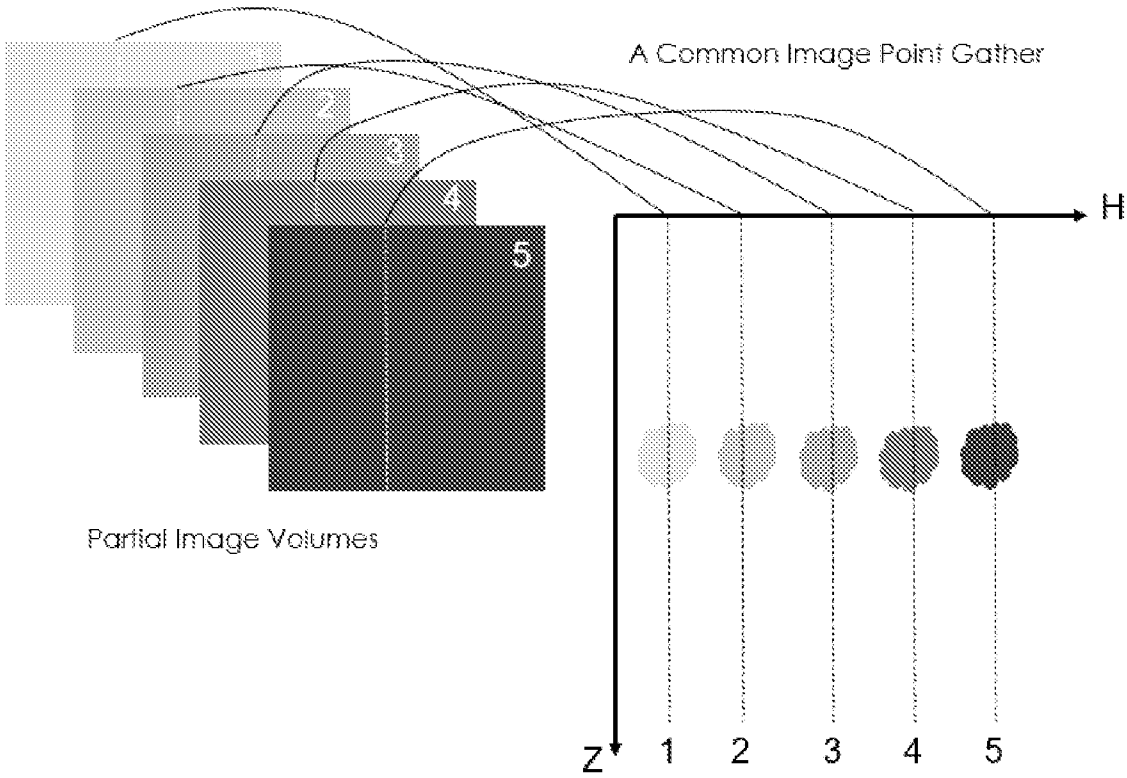
A Common Image Point Gather
1
2
3
4
5
H
Z
1
2
3
4
5
Partial Image Volumes

FIG. 2

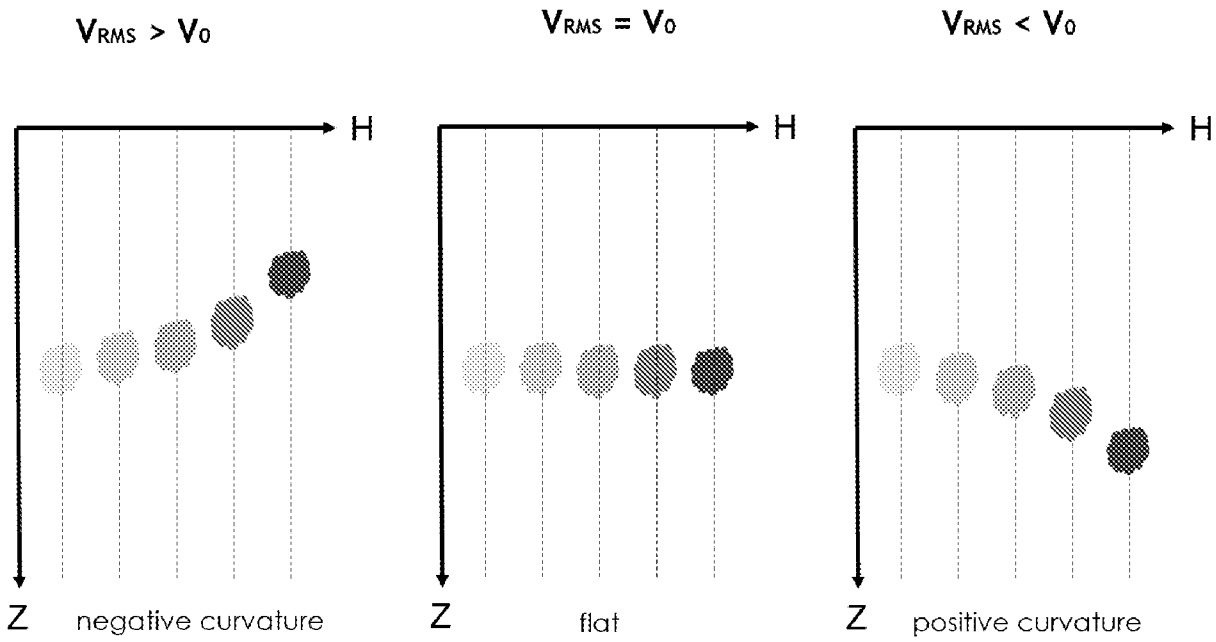
VRMS > V0
VRMS = V0
VRMS < V0
H
Z
negative curvature
flat
positive curvature

FIG. 3

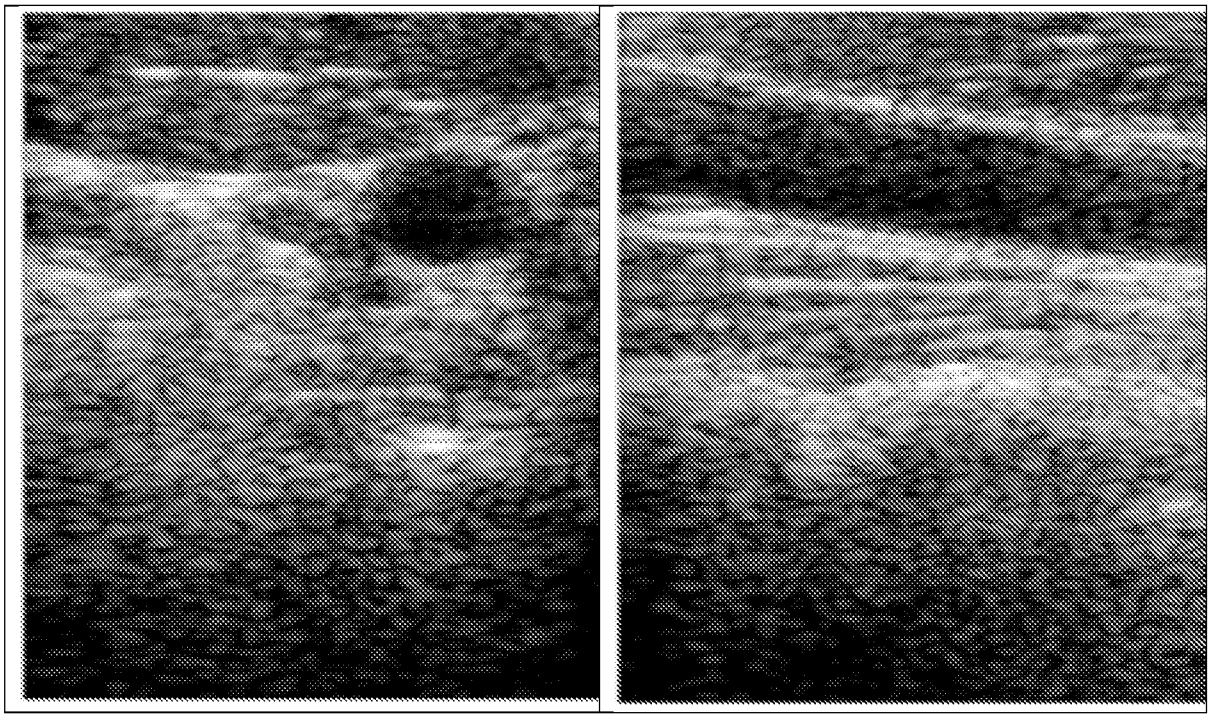

FIG. 4

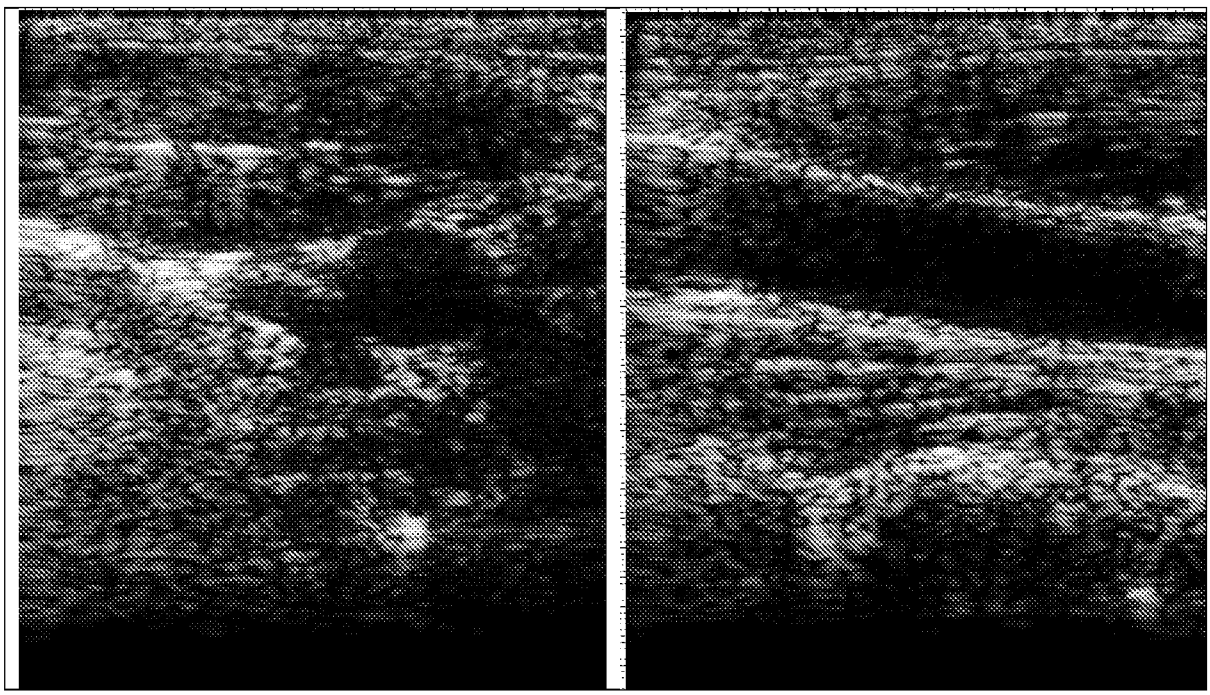

FIG. 5

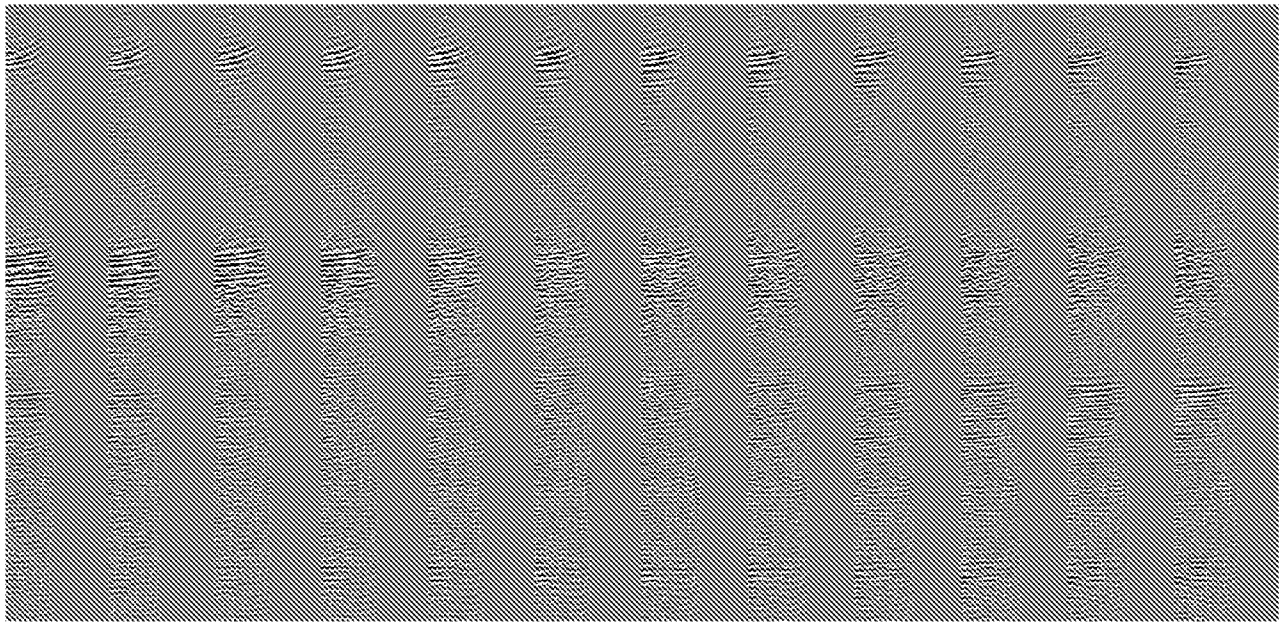

FIG. 6

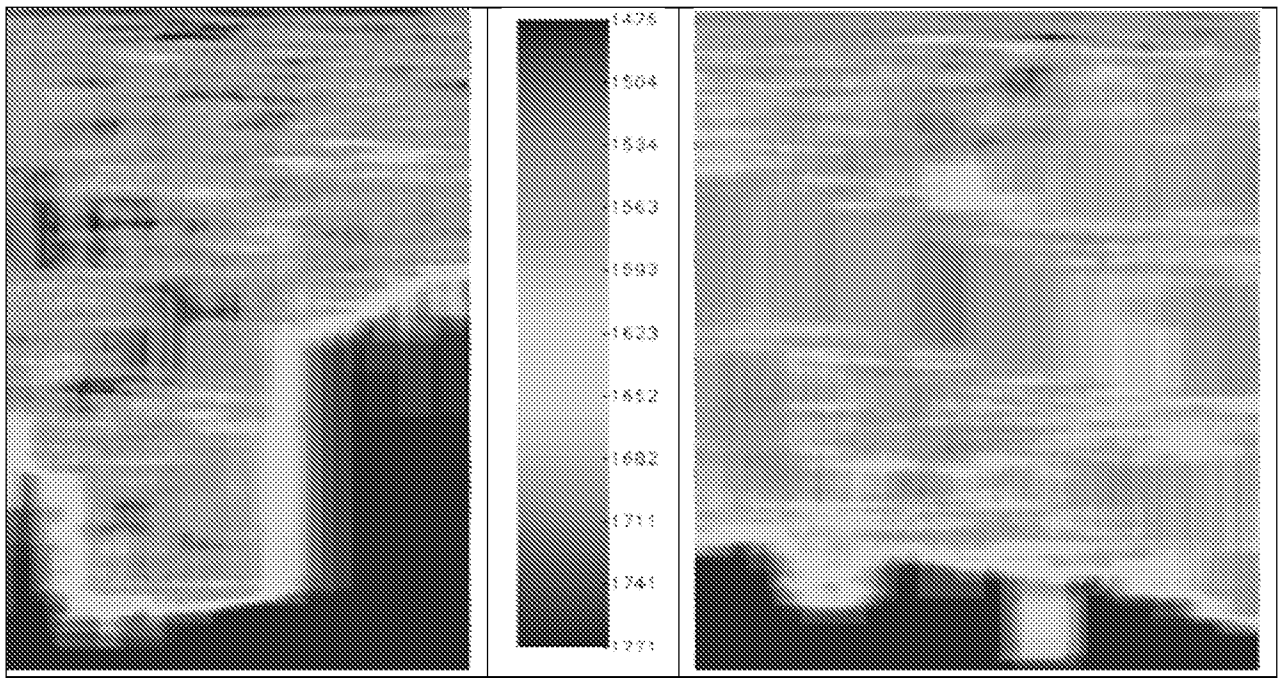

FIG. 7

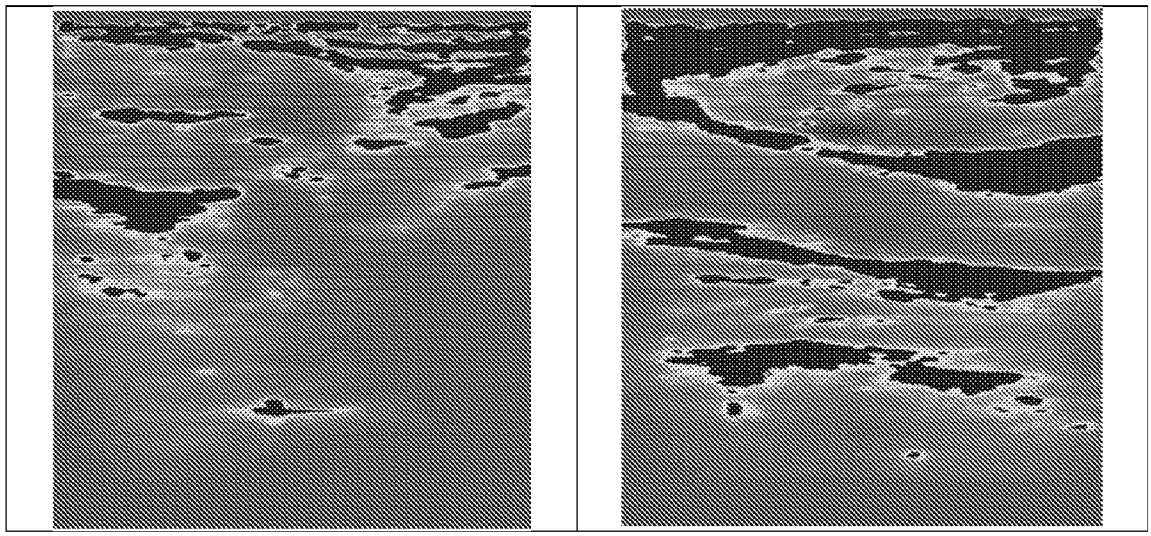

FIG. 8

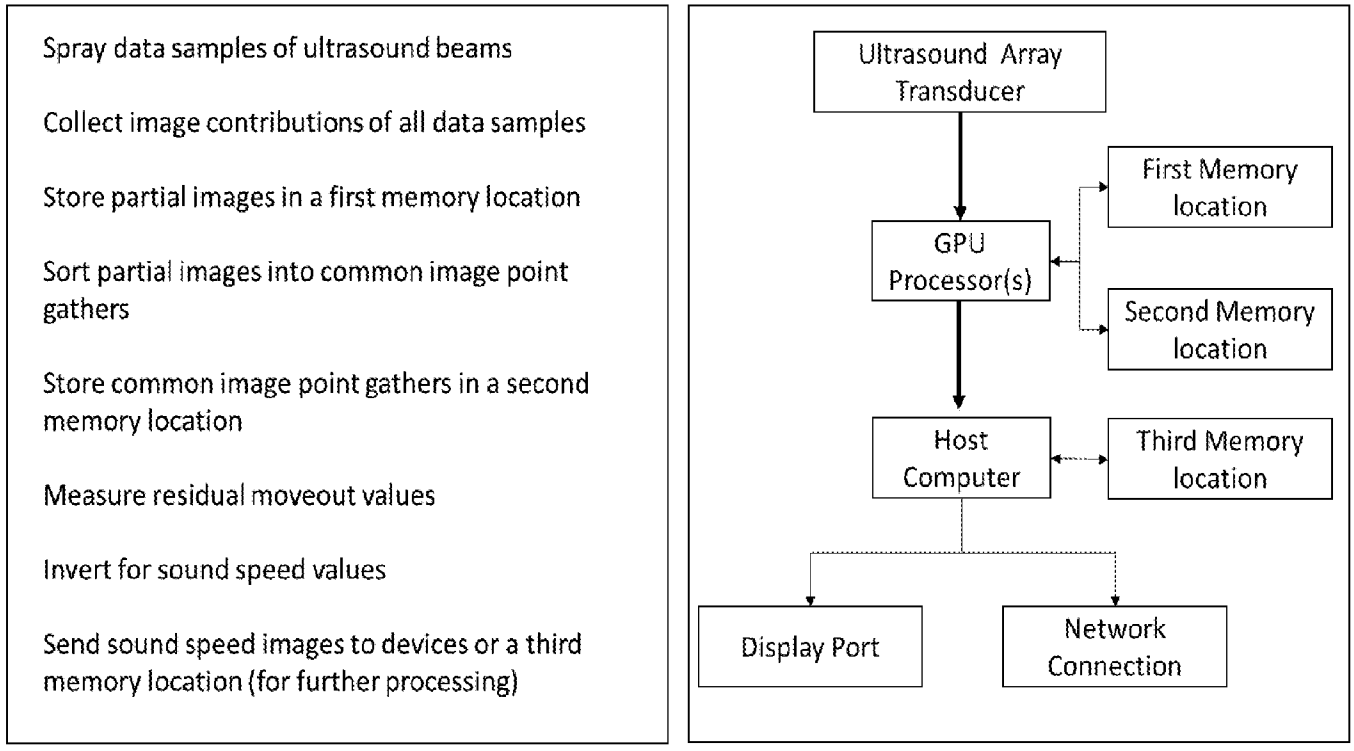
Spray data samples of ultrasound beams
Collect image contributions of all data samples
Store partial images in a first memory location
Sort partial images into common image point gathers
Store common image point gathers in a second memory location
Measure residual moveout values
Invert for sound speed values
Send sound speed images to devices or a third memory location (for further processing)
Ultrasound Array Transducer
First Memory location
GPU Processor(s)
Second Memory location
Host Computer
Third Memory location
Display Port
Network Connection
Data Processing Flow
Main Architecture of the Apparatus

FIG. 9

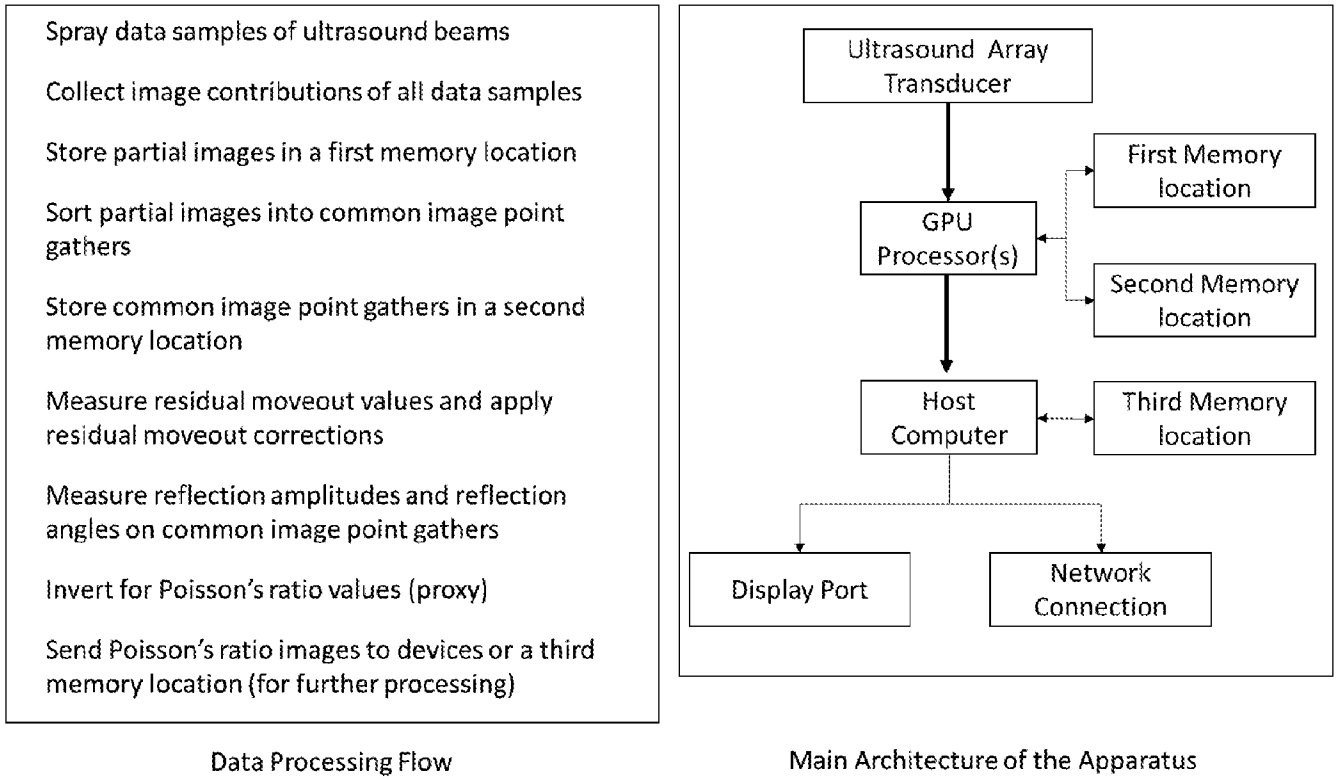
Spray data samples of ultrasound beams
Collect image contributions of all data samples
Store partial images in a first memory location
Sort partial images into common image point gathers
Store common image point gathers in a second memory location
Measure residual moveout values and apply residual moveout corrections
Measure reflection amplitudes and reflection angles on common image point gathers
Invert for Poisson's ratio values (proxy)
Send Poisson's ratio images to devices or a third memory location (for further processing)
Data Processing Flow
Ultrasound Array Transducer
First Memory location
GPU Processor(s)
Second Memory location
Host Computer
Third Memory location
Display Port
Network Connection
Main Architecture of the Apparatus

FIG. 10

INTERNATIONAL SEARCH REPORT

International application No.
PCT/US 22/39282

A. CLASSIFICATION OF SUBJECT MATTER

IPC - INV. G01S 15/89 (2022.01)
ADD. G01N 29/07 (2022.01)

CPC - INV. G01S 15/8963
ADD. G01N 29/07, G01S 7/52095, G01S 15/89, G01V 1/303

According to International Patent Classification (IPC) or to both national classification and IPC

B. FIELDS SEARCHED

Minimum documentation searched (classification system followed by classification symbols)
See Search History document

Documentation searched other than minimum documentation to the extent that such documents are included in the fields searched
See Search History document

Electronic data base consulted during the international search (name of data base and, where practicable, search terms used)
See Search History document

C. DOCUMENTS CONSIDERED TO BE RELEVANT

Category*	Citation of document, with indication, where appropriate, of the relevant passages	Relevant to claim No.
A	US 2007/0203673 A1 (SHERRILL et al.) 30 August 2007 (30.08.2007) Fig 3, 12, abstract, para [0002],[0004], [0046], [0048], [0049], [0125], [0130]	1-7
A	US 2009/0112093 A1 (BAE et al.) 30 April 2009 (30.04.2009) Fig 2, 3, abstract, para [0021]-[0023]	1-7
A	US 2020/0124752 A1 (BAUMSTEIN et al.) 23 April 2020 (23.04.2020) abstract, para [0030]	1-7

☐ Further documents are listed in the continuation of Box C. ☐ See patent family annex.

* Special categories of cited documents:
"A" document defining the general state of the art which is not considered to be of particular relevance
"D" document cited by the applicant in the international application
"E" earlier application or patent but published on or after the international filing date
"L" document which may throw doubts on priority claim(s) or which is cited to establish the publication date of another citation or other special reason (as specified)
"O" document referring to an oral disclosure, use, exhibition or other means
"P" document published prior to the international filing date but later than the priority date claimed
"T" later document published after the international filing date or priority date and not in conflict with the application but cited to understand the principle or theory underlying the invention
"X" document of particular relevance; the claimed invention cannot be considered novel or cannot be considered to involve an inventive step when the document is taken alone
"Y" document of particular relevance; the claimed invention cannot be considered to involve an inventive step when the document is combined with one or more other such documents, such combination being obvious to a person skilled in the art
"&" document member of the same patent family

Date of the actual completion of the international search	Date of mailing of the international search report
10 October 2022	OCT 28 2022
Name and mailing address of the ISA/US Mail Stop PCT, Attn: ISA/US, Commissioner for Patents P.O. Box 1450, Alexandria, Virginia 22313-1450 Facsimile No. 571-273-8300	Authorized officer Kari Rodriquez Telephone No. PCT Helpdesk: 571-272-4300